JOURNAL OF AIRCRAFT
Vol. 35, No. 4, July–August 1998

Vortex-Generator Installation Studies on Steady-State and Dynamic Distortion

Bernhard H. Anderson*
NASA Lewis Research Center, Cleveland, Ohio 44135
and
James Gibb†
Defence Research Agency, Bedford MK416AE, England, United Kingdom

The theoretical and experimental work carried out under the NASA/MOD joint aeronautical program has shown that computational fluid dynamics (CFD) vortex-generator installation designs successfully managed inlet-duct flow distortion and that significant benefits in flow unsteadiness at the engine face were also present. The main conclusions to date from the collaborative effort between the NASA Lewis Research Center and the Defence Research Agency in Bedford are as follows: 1) Vortex-generator installations can be designed to be effective over a wide range of inlet operating conditions using CFD and formal optimization procedures, 2) reductions in steady-state engine face distortion of up to 80% have been measured in the M2129 inlet S-duct using CFD-designed vortex-generator installations, 3) reductions in flow unsteadiness of up to 80% have been measured in the M2129 inlet S-duct using CFD-designed vortex-generator installations, and 4) the reduced Navier–Stokes code RNS3D is a useful tool to design vortex-generator installations to manage engine-face distortions over a wide range of inlet operating conditions.

Nomenclature

A = flow area
c = vortex-generator chord length
D = diameter
DC_{60} = circumferential total-pressure distortion descriptor
d = vortex-generator lateral spacing
h = vortex-generator blade height
M = Mach number
Pt = total pressure
Pt_{av} = average total pressure
Pt_{max} = maximum ring total pressure
Pt_{min} = 60 deg-sector minimum ring total pressure
Pt_0 = freestream or reference total pressure
Q = face-average dynamic pressure
R = radial distance
X = axial distance from inlet throat
α_{vg} = vortex-generator spacing angle
β_{vg} = vortex-generator incidence angle
δ_{ef} = dimensionless engine-face radial distance
δ^* = displacement thickness
θ_s = installation sector angle

Subscripts
ef = engine face
i = inlet-throat station
ring = ring
rms = total pressure RMS value
sep = separation
tip = tip
vg = vortex generators
0 = freestream or reference condition

Received April 3, 1996; presented as Paper 96-3279 at the AIAA/ASME/SAE/ASEE 32nd Joint Propulsion Conference, Lake Buena Vista, FL, July 1–3, 1996; revision received Jan. 30, 1998; accepted for publication Feb. 3, 1998.

*Senior Research Scientist.
†Senior Research Engineer.

Introduction

ENGINE-face distortion is one of the most troublesome and least-understood problems for designers of modern engine-inlet systems.[1,2] One issue is that there are numerous sources of flowfield distortion that are ingested by the inlet or generated within the inlet duct itself. Among these sources are 1) flow separation at the cowl lip during maneuvering flight, 2) flow separation on the compression surfaces because of shock-wave boundary-layer interactions, 3) spillage of the fuselage boundary layer into the inlet duct, 4) ingestion of aircraft vortices and wakes emanating from upstream disturbances, and 5) secondary flow and possibly flow separation within the inlet duct itself. Most developing aircraft have experienced one or more of these types of problems, particularly at high Mach numbers and/or extreme maneuver conditions, such that flow distortion at the engine face exceeded the allowable limits of the engine. Such inlet–engine compatibility problems were encountered in the early versions of the B70, F-111, F-14, MIG-25, Tornado, and Airbus A300.

The most common method of flow control in inlet ducts has been the inclusion of vane-type vortex generators, the application of which is an extension of design methods used in external aerodynamics to "locally" control the effects of separation. This is achieved by locally mixing the low- and high-momentum regions in the flow that effectively spreads out the lower-momentum fluid, thus suppressing separation. However, engine-face distortion is not often significantly reduced in three-dimensional inlet S-ducts, and the local use of generators only allows the separation to be controlled at one flow condition (usually the cruise condition), with all other flow conditions being "off-design."

The use of vortex generators within this study is viewed in an entirely different manner, i.e., the generators are used to "globally" restructure secondary flow for the purpose of increasing inlet total pressure recovery and decreasing engine-face distortion. The use of vortex generators as a global

method of secondary flow control was first proposed in Anderson et al.,[3] for the re-engining program on the 727-100 center inlet duct using the TAY650 series engine, and in Anderson and Gibb,[4] for the Defence Research Agency (DRA) M2129 inlet S-duct. As a consequence of this concept, vortex-generator installations can be optimized in terms of the inlet total pressure recovery and engine-face distortion level over a wide range of inlet operating conditions. It is not a design criterion to prevent flow separation unless it produces an overall improvement in engine-face flow characteristics. Therefore, the use of vortex generators as a global method of secondary flow control allows for the formal application of computational fluid dynamics (CFD) and numerical optimization procedures to vortex-generator installation design while encompassing a wide variety of inlet operating conditions.

The overall objectives of this study are to advance the understanding, prediction, and control of inlet distortion, and to study the basic interactions that influence this important design problem. Early findings from this research have been reported and demonstrate that CFD vortex-generator installation designs can manage secondary flow and, therefore, represent a control method to suppress engine-face, steady-state distortion.[4–6] However, these early results indicated that maximum reductions in DC_{60} engine-face distortion were not achieved because of the incorrect CFD prediction of the M2129 separation characteristics and the subsequent misplacement of the generator installation. The follow-on work under the NASA/MOD joint aeronautical program involved new CFD vortex-generator installation designs based on the experimental separation characteristics measured in the DRA/Bedford 13 × 9 ft wind tunnel. This paper describes the latter findings and focuses on both the calculated and experimental performance results of the new CFD-designed vortex-generator installations for the DRA M2129 inlet S-duct.

Theoretical Background

Three-dimensional viscous subsonic flows in complex inlet duct geometries are investigated by a numerical procedure that allows solution by spatial forward-marching integration, utilizing flow approximations from the velocity-decomposition approach of Briley and McDonald.[7,8] The goal of this approach is to achieve a level of approximation that will yield accurate flow predictions, while reducing the labor below what is needed to solve the full Navier–Stokes equations. The governing equations for this approach have been given previously for orthogonal coordinates, and the approach has been applied successfully to problems whose geometries can be fitted conveniently with orthogonal-coordinate systems. However, geometries encountered in typical subsonic inlet ducts cannot be treated easily using orthogonal coordinates, and this led to an extension of this approach by Levy et al.,[9] to treat ducted geometries with nonorthogonal coordinates. In generalizing the geometry formulation, Anderson[10] extended the analysis to cover ducted geometries defined by an externally generated grid file, such that it allowed for 1) reclustering the existing grid file, 2) redefining the centerline space curve, and 3) altering the cross-sectional shape and area distribution without modifying the original grid file. This version of the three-dimensional reduced Navier–Stokes computer code is called RNS3D. The turbulence model used in RNS3D is that of McDonald and Camarata,[11] which employes an eddy–viscosity formulation for the Reynolds' stresses.

The analysis as presented here is applicable only when the primary velocity is not negative. Because small regions of reverse flow can arise in curved inlet ducts, the numerical method is locally modified to permit forward marching when the flow contains small regions of reverse flow. The technique used follows Reyhner and Flugge-Lotz,[12] by adding small artificial convection at grid points where the primary flow is reversed. This is known as the FLARE approximation, after the authors.[12] For thin regions of reverse flow, although the streamwise extent of flow separation can be very large compared to the length of the passage, the technique permits the analysis to proceed downstream beyond reattachment, confining the FLARE approximation to the separated region. The use of parabolized equations to treat separated flow of the type experienced in the M2129 inlet S-duct was investigated experimentally by Whitelaw and Yu,[13] and computationally by Anderson and Farokhi[14] and Anderson et al.[15] The vortex-generator model that was used in this study was described by Kunik,[16] and has demonstrated "good qualitative agreement with idealized and experimental results." The vortex generators are modeled as a spatial distributed step increase in vorticity within the governing equation.

Results and Discussion

Experimental measurements were made on the ejector-driven M2129 inlet S-duct shown installed in the DRA/Bedford 13 × 9 ft wind tunnel in Fig. 1. These tests were made using the configuration corresponding to the AGARD FDP working group 13 test case 3, defined by Willmer et al.[17] The original lip no. 4 and forward extension no. 3 were used for this study. The S-duct section of the M2129 inlet model was split along the axis of symmetry to facilitate fitting a variety of vortex-generator configurations. The CFD analysis of the M2129 inlet S-duct was performed using RNS3D, and used a polar grid topology that consisted of 49 radial, 49 circumferential, and 107 streamwise nodal points to model the half-plane duct, for a total number of 256,907 grid points, (Fig. 2). The CPU time was 6.3 min on the Cray Y-MP for this computational grid. This large number of grid points was chosen to resolve the small interactions that are characteristic of vortex-generator flowfields. The internal grid was constructed such

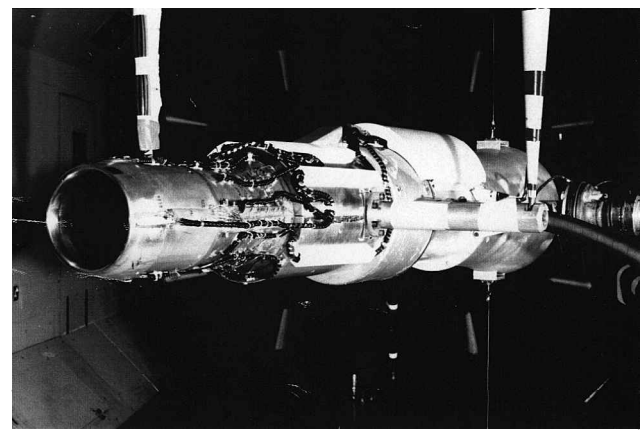

Fig. 1 M2129 inlet S-duct installed in the DRA/Bedford 13 × 9 ft wind tunnel.

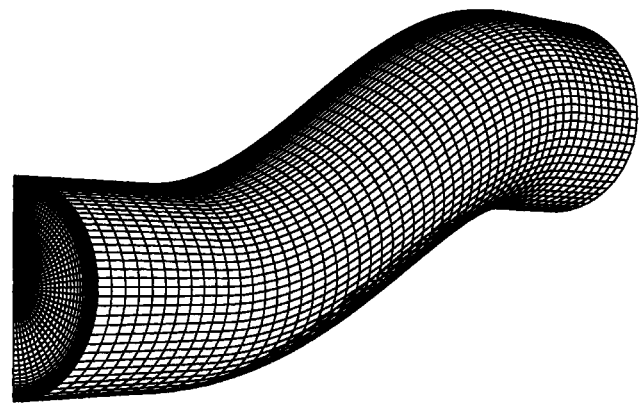

Fig. 2 Geometry and grid definition for the M2129 inlet S-duct, $L/R_i = 7.10$, $A_{ef}/A_i = 1.40$, $\Delta Z/R_i = -2.13$, grid = 49 × 49 × 107 = 256,907.

that the transverse computational plane was perpendicular to the duct centerline. Grid clustering was used in the radial direction to resolve the high-shear regions near the walls. The flow in the inlet duct was considered turbulent throughout. The inflow boundary-layer condition corresponds to a displacement thickness ratio, δ^*/R_i, of 0.018, and was applied two inlet radii, R_i, upstream of the inlet throat in the no. 3 forward constant area extension. This boundary-layer displacement thickness was chosen to provide the experimental inlet throat-corrected weight-flow values of 26.68 and 17.89 lb/s at the AGARD test case 3.1 and 3.2 conditions, respectively.

The relative engine-face distortion levels at different flight conditions are important because inlets must be designed to operate with low distortion over a flight envelope. Tradeoffs between what is needed at one flight condition (such as takeoff) and what is needed at other flight conditions (such as transonic maneuvering at low altitudes, or cruise) must be made. Mach number, Reynolds number, inlet-corrected weight flow, and engine tolerance can all change from one operating condition to another. It is, however, not necessary to solve the entire vortex-generator optimization problem by varying every design parameter over the flight envelope of interest. Aspects of the generator-installation design can and should be enhanced by a numerical optimization strategy. For example, in the present study, the vortex-generator geometric angle of incidence β_{vg}, and height-to-chord ratio h/c, were held fixed at 16.0 deg and 0.250, respectively. Two fixed vortex-generator installation locations, X_{vg}/R_i, were also chosen in the M2129 inlet S-duct at 1.0 and 2.0 R_i downstream of the inlet throat. (The significance of these two installation locations will be discussed in detail later in this paper.) Therefore, the optimization process involves the vortex-generator height ratio h/R_i, and the installation parameters of a number of corotating vortex generator pairs n_{vg}, angular spacing between vortex generators α_{vg}, and the angular extent of the installation θ_s, which

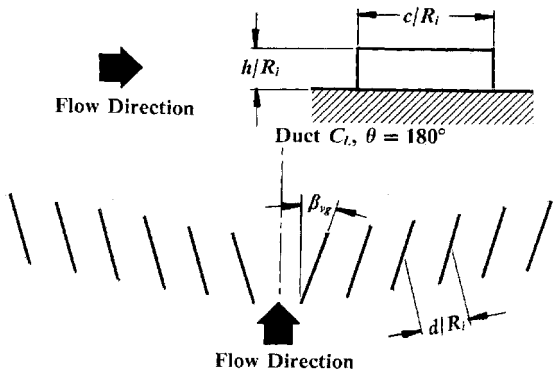

Fig. 3 Geometry definition for corotating vortex generators.

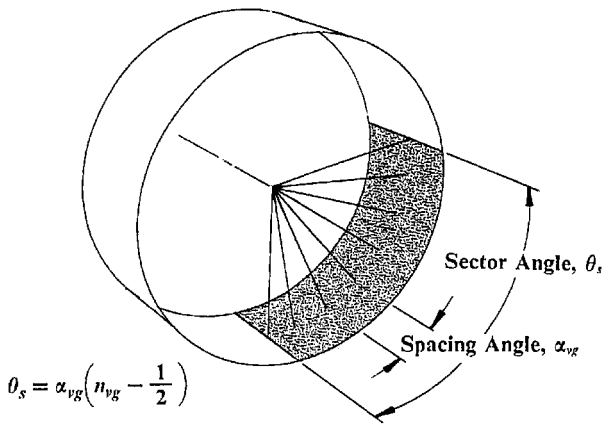

Fig. 4 Nomenclature used for vortex-generator positioning.

are all interrelated. These design parameters are defined in Figs. 3 and 4.

Selection of the performance parameter used to make judgments about the value of the generator installation is particularly interesting for three reasons. First, the required distortion level can be different at each important flight condition. Second, distortions levels greater than the engine tolerance are unacceptable, whereas distortion levels less than the engine tolerance are of little value other than being less than the engine distortion tolerance. Third, the engine itself must be defined because distortion descriptors are tied to a particular engine: There are no universal distortion descriptors. The importance of the engine-face distortion descriptor lies in the fact that the final vortex-generator installation that is acceptable will depend not only on the choice of descriptor, but also on how that descriptor is determined. For examples, in this study the DC_{60} distortion descriptor will take on significantly different values, depending whether this parameter is determined from an integration of data on the computational mesh or whether a 72-probe interpolated data set was used with the experimental DC_{60} data-reduction package. Therefore, the calculated inlet total pressure recovery levels and the distortion levels presented in this study were based on the same data-reduction routines as used in the DRA/Bedford experiments. The engine-face flow unsteadiness parameter Pt_{rms}/Q presented in this paper was based on the average rms value of eight pressure transducers spaced 45 deg apart and located at 67% of the engine-face radius.

Each of the locally optimum vortex-generator installations provided by NASA Lewis Research Center was determined using numerical optimization techniques; however, only the vortex-generator installation located two R_i downstream of the inlet throat will be described in this paper. Both the engine-face total pressure recovery Pt_{av}/Pt_0 and DC_{60} levels were monitored during the optimization process; however, the total pressure recovery optimization characteristics are not presented here for the purpose of brevity. The design process begins using an installation composed of 11 corotating vortex-generator pairs, each with an angular lateral spacing of 15.0 deg and distributed over a sector angle of 157.5 deg within the M2129 inlet S-duct. It does not matter which vortex generator configuration is used as the starting installation as long as the optimization process is completed. The standard blade section used in this study was composed of a low-aspect ratio, flat-plate, vane-type generator, where the aspect ratio h/c was set at 0.250 and the β_{vg} was set at 16.0 deg for all configurations. It should be remembered that only a half-duct calculation was performed in this study; therefore, the total number of vortex generators in the experimental duct was twice the number of generators used in the computational S-duct. Also, the other half of the M2129 inlet S-duct is the mirror image of the computational S-duct. Therefore, each corotating generator can be viewed as having a corresponding mirror image, i.e., the corotating generators can be labeled as pairs. A series of calculations using RNS3D were performed over a range of vortex-generator blade heights h/R_i from 0.050 to 0.080 for inlet-throat Mach-number conditions of 0.794 and 0.412. These inlet operating conditions correspond to the AGARD FDP working group 13 test cases 3.1 and 3.2, respectively. The effect of generator blade height on DC_{60} engine-face distortion is presented in Fig. 5 and indicates that a blade height of 0.070 would provide the lowest overall distortion level over the nominal inlet-throat Mach number range from 0.4 to 0.8. Although the design objective was to optimize over the nominal throat Mach number range from 0.2 to 0.8, experience has demonstrated that it is not necessary to consider inlet-throat Mach numbers below 0.4 for this type of study. To demonstrate that this vortex-generator installation indeed represents a "local optimum" configuration, a series of calculations were performed over a range of generator sector angles from 0.0 to 157.5 deg (at a fixed spacing angle of 15.0 deg) (Fig. 6), as

Table 1 Matrix of CFD-designed vortex-generator installations tested in the Bedford 13 × 9 ft wind tunnel

Designation	VG130	VG160	VG165	VG170
Number of pairs, n_{vg}	11	13	11	11
Sector location, X_{vg}/R_i	3.0	1.0	1.0	2.0
Blade height, h/R_i	0.075	0.060	0.065	0.070
Chord length, c/R_i	0.300	0.240	0.260	0.280
Lateral spacing, d/R_i	0.289	0.224	0.267	0.277
Spacing angle, α_{vg}, deg	15.0	12.6	15.0	15.0
Angle of incidence, β_{vg}, deg	16.0	16.0	16.0	16.0
Sector angle, θ_s, deg	157.5	157.5	157.5	157.5

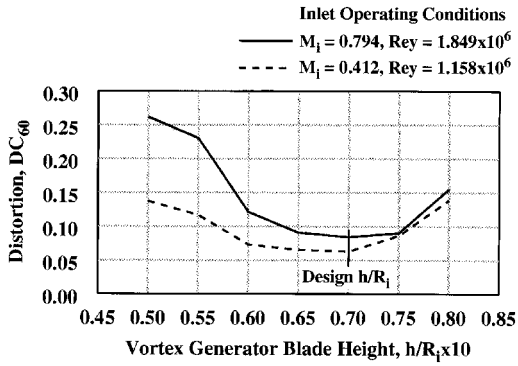

Fig. 5 Effect of vortex-generator blade height on DC_{60} engine-face, steady-state distortion.

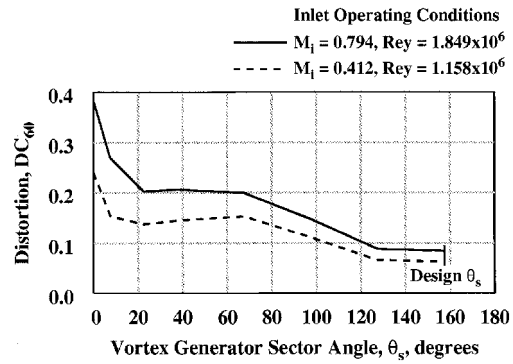

Fig. 6 Effect of vortex-generator sector angle on DC_{60} engine-face, steady-state distortion, generator spacing angle α_{vg} = 15.0 deg.

well as a range of spacing angles from 12.6 to 63.0 deg (at a constant sector angle of 157.0 deg) (Fig. 7). These results substantiated that the sector angle of 157.5 deg and spacing angle of 15.0 deg provided the lowest overall distortion level over the nominal inlet-throat Mach-number range from 0.2 to 0.8. This vortex-generator installation was labeled as VG170. In a similar manner, vortex-generator installations VG160 and VG165 were also determined to be locally optimum configurations.

The matrix of CFD-designed vortex-generator installations tested in the DRA/Bedford 13 × 9 ft wind tunnel are presented in Table 1. The important geometric parameters for vortex-generator installation design includes 1) the number of vortex-generator pairs n_{vg}; 2) the generator sector axial location X_{vg}/R_i; 3) the vortex-generator blade height h/R_i; 4) the vortex-generator chord length c/R_i; 5) the lateral spacing between generator blades d/R_i; 6) the lateral spacing angle α_{vg}, which is equivalent to the lateral spacing parameter d/R_i; 7) the vortex-generator blade angle-of-incidence β_{vg}; and 8) the installation sector angle θ_s, which is a function of both the number of vortex-generator pairs n_{vg} and generator spacing angle α_{vg}. There can be many more vortex-generator design parameters. For example, it may be advantageous to vary the height of the

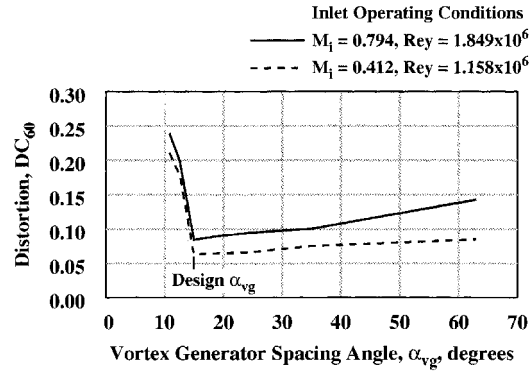

Fig. 7 Effect of vortex-generator spacing angle on DC_{60} engine-face, steady-state distortion, generator sector angle θ_s = 157.5 deg.

generator blades in the circumferential direction, or to have more than one generator-installation location, or to use a mix of counterrotating and corotating vortex generators. It should be restated that it is not necessary to solve the entire vortex-generator optimization problem using all of the design parameters over the flight envelope of interest. Aspects of the generator-installation design can and should be enhanced by a numerical-optimization strategy based on a common-sense understanding of how vortex generators operate as an installation. Figure 8 shows a half-plane schematic illustration of vortex-generator configuration VG170 installed in the DRA M2129 inlet S-duct. The relationship between the location of the family of vortex-generator installations X_{vg}/R_i, presented in Table 1, and both the experimental and computed separation characteristics are presented in Fig. 9. Both full Navier–Stokes and reduced Navier–Stokes analysis of the separation characteristics were performed for the M2129 baseline S-duct inlet using algebraic turbulence models.[15] Vortex-generator configurations VG160 and VG165 were located within the M2129 S-duct at a one R_i downstream of the inlet throat such that the experimental flow separation encountered over the inlet Mach-number range tested was always downstream of the generator installation. Vortex-generator configuration VG170, however, was located at two R_i downstream of the inlet throat (Fig. 8). At this axial station the separation moved slightly into the generator region at the higher inlet-throat Mach-number flow regime (Fig. 9). Because the vortex generators in the good flow can still reverse the effects of secondary flow, acceptable performance can still be achieved. Vortex-generator installation VG130 was designed relative to computed separation characteristics, which were well downstream of the actual (experimental) separation characteristics. In the lower Mach-number range, this generator installation reduced DC_{60} engine-face distortion about 75%, while at the higher inlet-throat Mach-number region, only a 25% reduction in steady-state distortion was realized. Hence, this installation did not perform as well as desired, although these are remarkable performance gains for a vortex-generator installation located in the middle of a strongly separated flow region.

The vortex-generator configurations VG160, VG165, and VG170 that were tested all represent local optimum installation

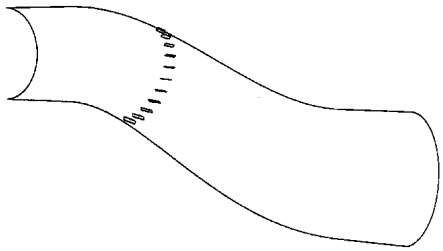

Fig. 8 Vortex-generator configuration VG170 installed in the DRA M2129 inlet S-duct.

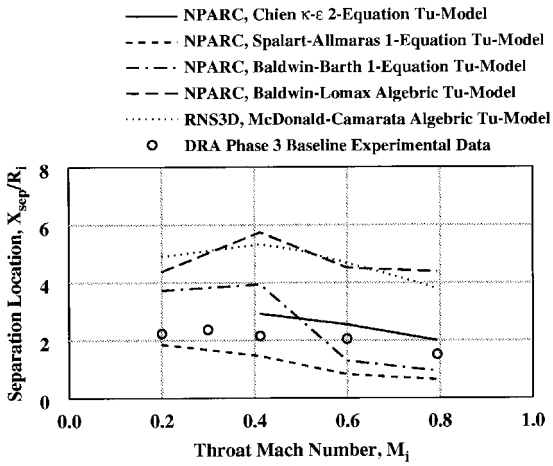

Fig. 9 Computed and measured separation characteristics in the M2129 baseline inlet S-duct.

designs as obtained using RNS3D. Vortex-generators installations VG160 and VG165 were located at an axial position one R_i downstream of the inlet throat, which was always upstream of the most forward-flow separation (vortex liftoff) location measured over the throat Mach-number range tested. The generator installations VG160 and VG165 differed in the number of vortex-generator pairs, the vortex-generator blade height, and both lateral and angular spacing (Table 1). The performance of vortex-generator installations VG160 and VG165, including a comparison between the calculated and measured engine-face flowfields, are presented in Figs. 10–17. Figure 10 shows the overall effect of vortex-installation VG160 on the inlet total pressure recovery Pt_{av}/Pt_0 (Fig. 10a), the DC_{60} steady-state engine-face distortion (Fig. 10b), and the rms of total pressure fluctuations Pt_{rms}/Q at the engine face (Fig. 10c), as compared to the baseline or empty M2129 inlet duct. The benefits in total pressure recovery, engine-face steady-state distortion, and engine-face total pressure fluctuations as a consequence of vortex installation VG160 are clearly seen. When the effects of generator-installation VG160 are compared to the empty or baseline performance, reductions in engine-face distortion of nearly 80% were realized. Comparing the calculated (solid and dashed lines) with the experimental (circular and square symbols) inlet performance indicates very good agreement in predicting total pressure recovery, but it indicated an overprediction of the effect of generator installation VG160 on DC_{60} engine-face distortion at the higher inlet-throat Mach numbers (Fig. 10b). Figures 11–14 present a comparison between the calculated and measured engine-face total pressure recovery contours at a nominal inlet throat Mach number of 0.4 and 0.8 for both the baseline S-duct (Figs. 10 and 11), as well as for vortex-generator installation VG160 (Figs. 13 and 14). A comparison between engine-face baseline recovery contours at nominal throat Mach numbers of 0.4 and 0.8 (Figs. 11 and 12), and the engine-face recovery contours for VG160 (Figs. 13 and 14), indicates that optimally designed vortex-generator installations tend to distribute the low-energy flow uniformly around the inside periphery of the engine face, leaving a high-energy core flow. In general, the agreement between analysis and measurement is quite good at both inlet-throat Mach numbers. However, at a nominal inlet-throat Mach number of 0.8, the measured engine-face total-pressure contours indicated a bad tube at the 90-deg rake location (Fig. 14). This bad tube reading, the effect of which tended to increase with increasing inlet-throat Mach number, was included in the DC_{60} measured distortion results, and could clearly explain the difference between the calculated and measured distortion presented in Fig. 10b. Very similar performance improvements were obtained with vortex-generator installation VG165 relative to the baseline S-duct performance (Fig. 15). Again, the agreement between analysis and measurements was very good, except for the tendency to overpredict the effect of VG165 on DC_{60} steady-state engine-face distortion (Fig. 14b), at the

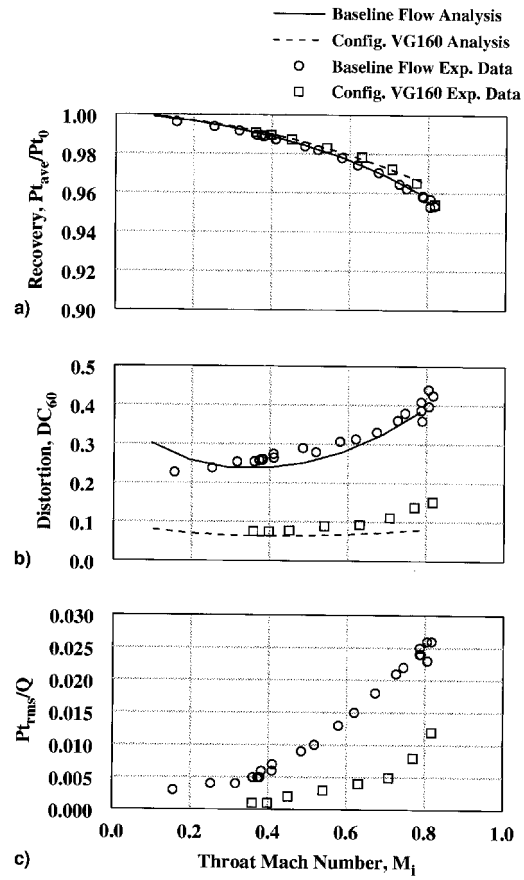

Fig. 10 Effect of vortex-generator configuration VG160 on the M2129 inlet S-duct performance: a) engine-face total pressure recovery, b) engine-face DC_{60} steady-state distortion, and c) engine-face Pt_{rms}/Q unsteady distortion.

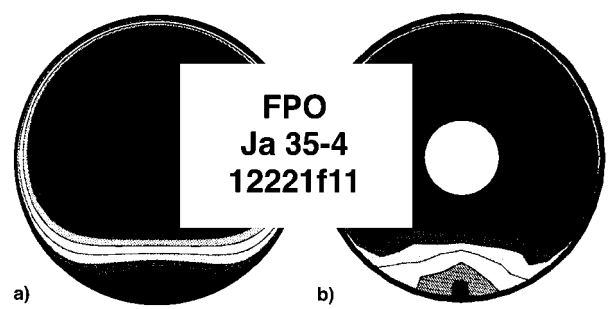

Fig. 11 Comparison of calculated and experimental engine-face total pressure recovery contours for the M2129 baseline flow, nominal throat Mach number M_i = 0.4: a) NASA Lewis Research Center's RNS3D analysis and b) DRA/Bedford experimental data.

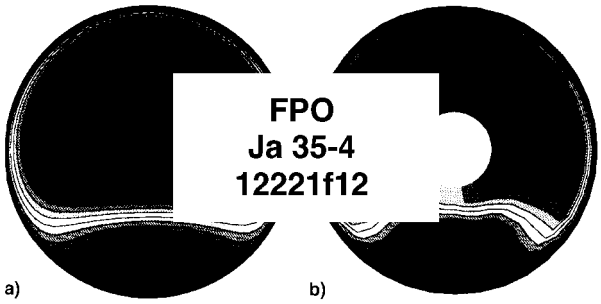

Fig. 12 Comparison of calculated and experimental engine-face total pressure recovery contours for M2129 baseline flow, nominal throat Mach number M_i = 0.8: a) NASA Lewis Research Center's RNS3D analysis and b) DRA/Bedford experimental data.

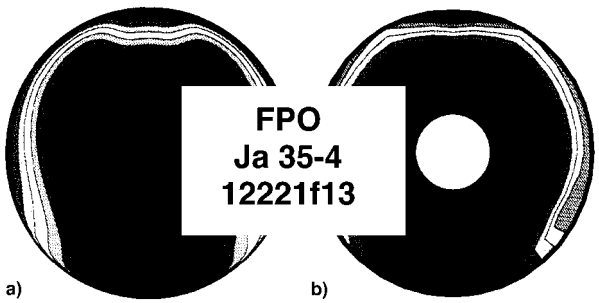

Fig. 13 Comparison of calculated and experimental engine-face total pressure recovery contours for generator configuration VG160, nominal throat Mach number M_i = 0.4: a) NASA Lewis Research Center's RNS3D analysis and b) DRA/Bedford experimental data.

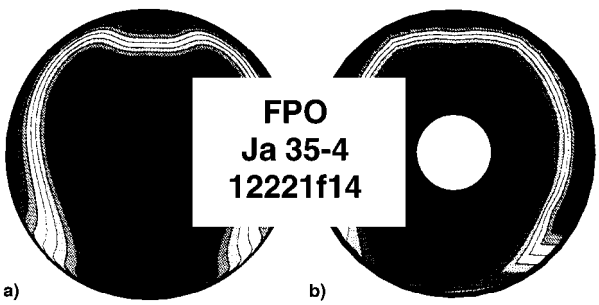

Fig. 14 Comparison of calculated and experimental engine-face total pressure recovery contours for generator configuration VG160, nominal throat Mach number M_i = 0.8: a) NASA Lewis Research Center's RNS3D analysis and b) DRA/Bedford experimental data.

higher inlet-throat Mach numbers. However, the same bad tube reading was still present in the measured VG165 engine total-pressure results (Figs. 16 and 17).

Vortex-generators installation VG170 was located two R_i downstream of the inlet throat (Fig. 8). At this generator-installation location, the separation was slightly downstream of the generators at the lower inlet-throat Mach numbers, but slightly upstream at the higher inlet-throat Mach numbers (Fig. 9). Figure 18 presents the effects of vortex-generator configuration VG170 on the inlet total pressure recovery (Fig. 18a), the DC_{60} steady-state engine-face distortion (Fig. 18b), and the rms of total pressure fluctuations Pt_{rms}/Q at the engine face (Fig. 18c). The results of the RNS3D analysis and DRA experiments on the VG170 vane-type generator installation are compared with the M2129 empty baseline S-duct flow. The benefits in total pressure recovery, engine-face steady-state distortion, and engine-face total pressure fluctuations are clearly seen. When the effect of the vane-type vortex generators are compared to the empty baseline performance, reduction distortions of nearly 80% are realized at the higher inlet-throat

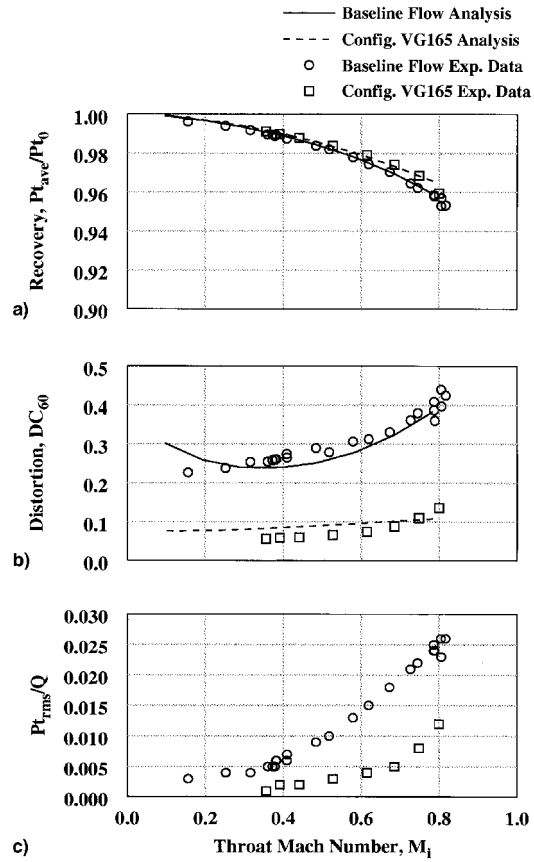

Fig. 15 Effect of vortex-generator configuration VG165 on the M2129 inlet S-duct performance: a) engine-face total pressure recovery, b) engine-face DC_{60} steady-state distortion, and c) engine-face Pt_{rms}/Q unsteady distortion.

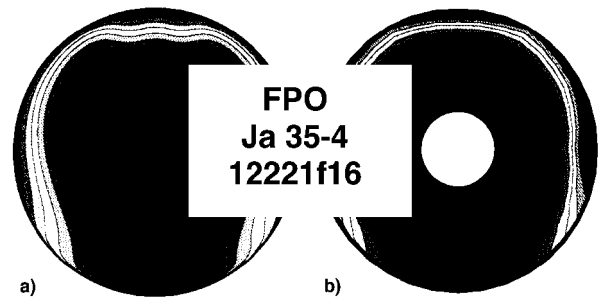

Fig. 16 Comparison of calculated and experimental engine-face total pressure recovery contours for generator configuration VG165, nominal throat Mach number M_i = 0.4: a) NASA Lewis Research Center's RNS3D analysis and b) DRA/experimental data.

Mach numbers. Similar percentage reductions in engine-face distortion can be seen at the lower inlet-throat Mach numbers, but here the lower baseline S-duct distortions are less of a problem. This is true for the RNS3D analysis prediction (solid and dashed lines) and DRA experimental results (circular and square symbols) of the baseline empty S-duct and vortex-generator configuration VG170, which are in remarkably good agreement. A further benefit of the global approach to vortex-generator installation design is that the generators themselves can be partially located in the separation region, as is the case with the VG170 installation at the high inlet-throat Mach numbers. Because the vortex generators in the good flow can still reverse the effects of secondary flow, very acceptable performance was achieved. In fact, the performance results of configuration VG170 presented in Fig. 18 suggests that global

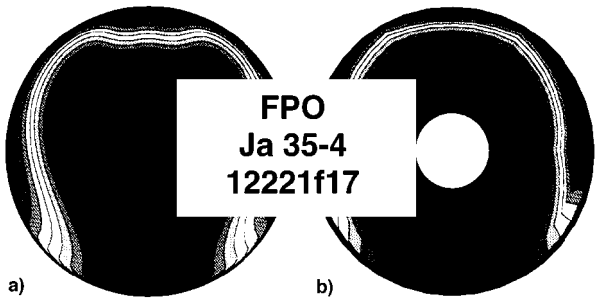

Fig. 17 Comparison of calculated and experimental engine-face total pressure recovery contours for generator configuration VG165, nominal throat Mach number M_i = 0.8: a) NASA Lewis Research Center's RNS3D analysis and b) DRA/Bedford experimental data.

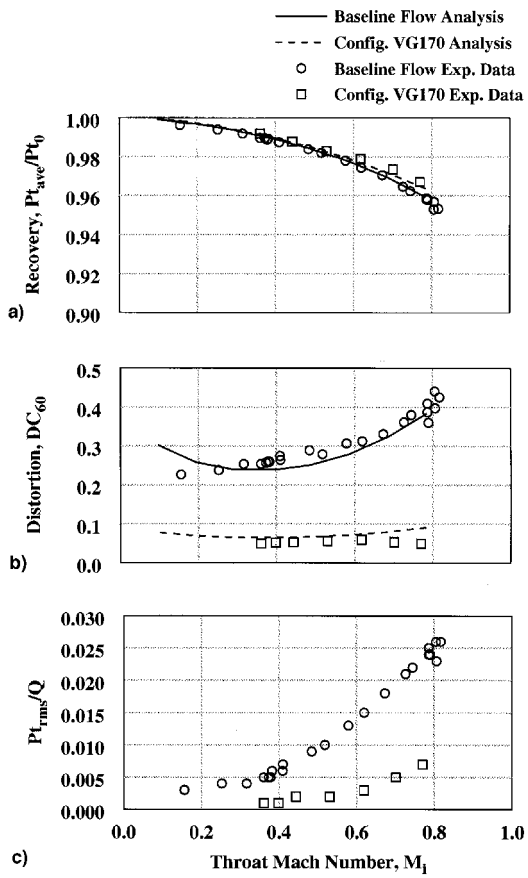

Fig. 18 Effect of vortex-generator configuration VG170 on the M2129 inlet S-duct performance: a) engine-face total pressure recovery, b) engine-face DC_{60} steady-state distortion, and c) engine-face Pt_{rms}/Q unsteady distortion.

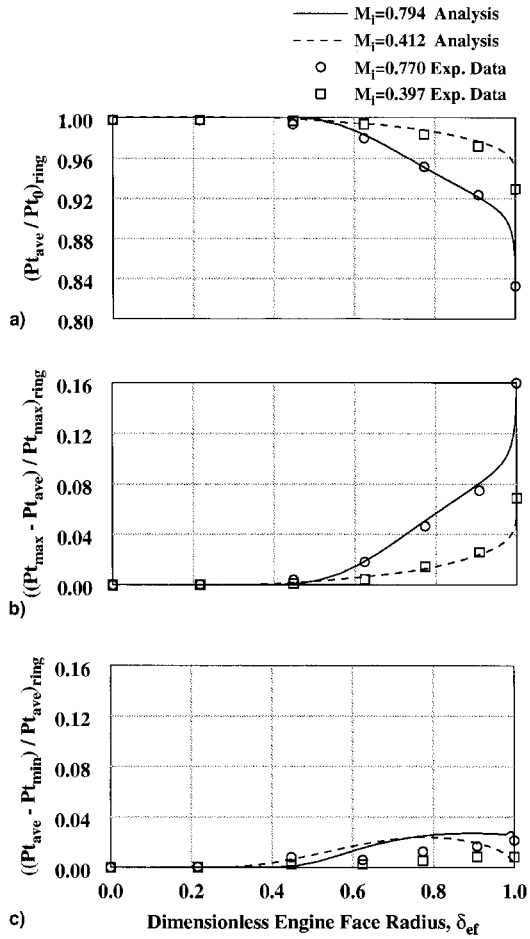

Fig. 19 Effect of vortex-generator configuration VG170 on the M2129 inlet S-duct engine-face distortion characteristics: a) engine-face ring total pressure recovery, b) engine-face radial ring distortion, and c) engine-face 60-deg sector circumferential ring distortion.

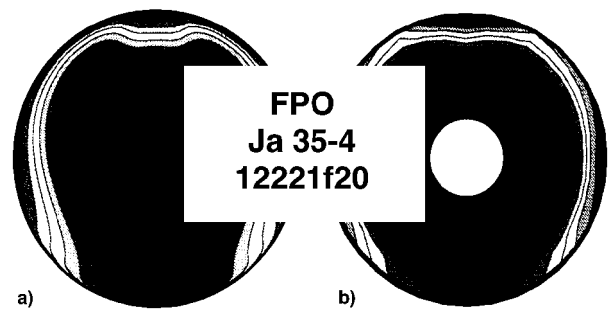

Fig. 20 Comparison of calculated and experimental engine-face total pressure recovery contours for generator configuration VG170, nominal throat Mach number M_i = 0.4: a) NASA Lewis Research Center's RNS3D analysis and b) DRA/Bedford experimental data.

management of partially separated or spoiled flow can even produce better overall optimum vortex-generator installation performance than the management of attached or unspoiled flow.

Figure 19 shows a comparison between the calculated and measured engine-face, ring-distortion descriptors at nominal inlet-throat Mach numbers of 0.4 and 0.8 for vortex-generator configuration VG170. These descriptors include the engine-face ring total pressure recovery distribution (Fig. 19a), the radial ring distortion (Fig. 19b), and the 60-deg sector circumferential ring distortion (Fig. 19c). The quantitative agreement between the RNS3D analysis and the DRA experimental is very good. A comparison between the calculated and measured engine-face total pressure recovery contours for vortex-generator configuration VG170 are presented in Figs. 20 and 21 for nominal inlet-throat Mach numbers of 0.4 and 0.8, respectively, and show good agreement. Likewise, a comparison between engine-face baseline recovery contours at nominal throat Mach numbers of 0.4 and 0.8 (Figs. 11 and 12), and the engine-face recovery contours for VG170 (Figs. 20 and 21), indicate that optimally designed vortex-generator installations tend to distribute the low-energy flow uniformly around the inside periphery of the engine face, leaving a high-energy core flow.

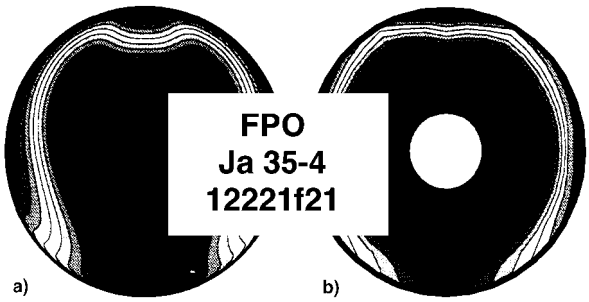

Fig. 21 Comparison of calculated and experimental engine-face total pressure recovery contours for generator configuration VG170, nominal throat Mach number M_t = 0.8: a) NASA Lewis Research Center's RNS3D analysis and b) DRA/Bedford experimental data.

Concluding Remarks

The vortex-generator configurations VG160, VG165, and VG170, that were tested under the NASA/MOD joint aeronautical program in the DRA/Bedford 13 × 9 ft wind tunnel, all represent local optimum installation designs as provided by NASA Lewis Research Center using RNS3D. The performance improvements realized over the baseline M2129 inlet S-duct for these three installation designs were as much as 80% reduction in steady-state DC_{60} engine-face distortion and 80% reduction in Pt_{rms}/Q engine-face dynamic distortion. It is also evident from the results presented in this paper that restructuring the secondary flow to maximize total pressure recovery and minimize engine-face DC_{60} distortion using optimization procedures has the effect of searching for a generator installation that distributes the low-energy flow uniformly around the inside periphery of the engine face, leaving a high-energy core flow. Lastly, the experimental data obtained at DRA/Bedford demonstrates conclusively that optimally designed vortex-generator installations using CFD can greatly suppress both steady-state and dynamic engine-face distortion.

The use of vortex generators as a global method of secondary flow control allowed for the formal application of optimization procedures to be used with RNS3D while encompassing a wide variety of inlet flow conditions. The vortex generators were optimized in terms of engine-face total pressure recovery Pt_{av}/Pt_0 and DC_{60} engine-face distortion levels from the M2129 inlet S-duct. It was not a design criterion to prevent separation unless it produced an overall improvement in the engine-face flow characteristics. A further benefit of the global approach to vortex-generator installation design is that the generators themselves can be partially located in the separation region, as is the case with the VG170 installation at the high inlet-throat Mach numbers. Because the vortex generators in the good flow can still reverse the effects of secondary flow, good performance was still achieved. In fact, the performance results of configuration VG170 suggest that global management of partially separated or spoiled flow can even produce better overall optimum vortex-generator installation performance than the management of attached flow.

The computer code used to design the vortex-generator installation presented in this paper was RNS3D. The vortex generators are not directly computed, but rather the effect of the vortex generator was fed in as a spatially distributed step increase in vorticity in the governing equations. There are two modeling issues related to this approach: 1) The form of the spatial vorticity signature created by the individual generators, and 2) the relationship between the physical geometry of the generators and the strength of vortex produced. Both of these issues are currently being studied, and improved vortex-generator modeling is underway in RNS3D. However, the overall agreement between analysis and experiment is excellent. This substantiates the use of vortex-generator models in reduced Navier–Stokes analyses as a valid approach to vortex-generator installation design, and suggests that this approach is also valid for full Navier–Stokes analysis.

References

[1]"Engine Response to Distorted Inflow Conditions," AGARD, CP-400, Sept. 1986.

[2]Bowditch, D. N., and Coltrin, R. E., "A Survey of Inlet/Engine Distortion Compatibility," AIAA Paper 83-1166, 1986.

[3]Anderson, B. H., Huang, P. S., Paschal, W. A., and Cavatorta, E., "Study of Vortex Flow Control of Inlet Distortion," *Journal of Propulsion and Power*, Vol. 8, No. 6, 1992, pp. 1266–1272.

[4]Anderson, B. H., and Gibb, J., "Study on Vortex Generator Flow Control for the Management of Inlet Distortion," *Journal of Propulsion and Power*, Vol. 9, No. 3, 1993, pp. 420–430.

[5]Gibb, J., and Jackson, M., "Some Preliminary Results from Tests Using Vortex Generators in the Circular/Circular Diffusing S-Duct Model M, Rept. AP4(92)WP15, Aug. 1992.

[6]Gibb, J., and Anderson, B. H., "Vortex Flow Control Applied to Aircraft Inlet Ducts," High Lift and Separation Control Conf., Univ. of Bath, Bath, England, UK, 1995.

[7]Briley, W. R., and McDonald, H., "Analysis and Computation of Viscous Subsonic Primary and Secondary Flow," AIAA Paper 79-1453, Jan. 1979.

[8]Briley, W. R., and McDonald, H., "Three-Dimensional Viscous Flows with Large Secondary Velocities," *Journal of Fluid Mechanics*, Vol. 144, March 1984, pp. 47–77.

[9]Levy, R., Briley, W. R., and McDonald, H., "Viscous Primary/Secondary Flow Analysis for Use with Nonorthogonal Coordinate Systems," AIAA Paper 83-0556, Jan. 1983.

[10]Anderson, B. H., "The Aerodynamic Characteristics of Vortex Ingestion for the F/A-18 Inlet Duct," AIAA Paper 91-0130, Jan. 1991.

[11]McDonald, H., and Camarata, F. J., "An Extended Mixing Length for Computing the Turbulent Boundary-Layer Development," *Proceedings of the Stanford Conference of Turbulent Boundary Layers*, Vol. 1, Stanford Univ., Stanford, CA, 1969, pp. 83–98.

[12]Reyner, T. A., and Flugge-Lotz, I., "Interaction of a Shock Wave with a Laminar Boundary Layer," *Internal Journal of Non-Linear Mechanics*, Vol. 3, 1968.

[13]Whitelaw, J. H., and Yu, S. C., "Velocity Measurements in an S-Shaped Duct," *Experiments in Fluids*, Vol. 15, 1993, pp. 364–367.

[14]Anderson, B. H., and Farokhi, S., "A Study of Three Dimensional Turbulent Boundary Layer Separation and Vortex Flow Control Using Reduced Navier-Stokes Equations," Turbulent Shear Flow Symposium, Munich, Germany, Sept. 1991.

[15]Anderson, B. H., Reddy, D. R., and Kapoor, K., "A Comparative Study of Full Navier-Stokes and Reduced Navier-Stokes Analyses for Separating Flows Within a Diffusing Inlet S-Duct," AIAA Paper 93-2154, June 1993.

[16]Kunik, W. G., "Application of a Computational Model for Vortex Generators in Subsonic Internal Flows," AIAA Paper 86-1458, June 1986.

[17]Willmer, A. C., Brown, T. W., and Goldsmith, E. L., "Effects of Intake Geometry on Circular Pitot Inlet Performance at Zero and Low Forward Speeds," *Aerodynamics of Power Plant Installation*, AGARD, CP301, Toulouse, France, May 1981, pp. 51–56 (Paper 5).

Color reproductions courtesy of NASA Lewis Research Center.